The Solution Structure of the DNA Double-Stranded Break Repair Protein Ku and Its Complex with DNA: A Neutron Contrast Variation Study†

Jinkui Zhao,‡,§ Jinting Wang,|| David J. Chen,|| Scott R. Peterson,|| and Jill Trewhella*,‡

Chemical Science & Technology and Life Sciences Divisions, Los Alamos National Laboratory, Los Alamos, New Mexico 87545

Received October 22, 1998; Revised Manuscript Received December 16, 1998

ABSTRACT: Small-angle X-ray and neutron scattering with contrast variation has been used to study the structure of the DNA targeting component (Ku) of the DNA-dependent protein kinase and its complex with DNA. The Ku protein in solution has the approximate shape of a prolate ellipsoid with semi-axes of 24, 43, and 89 Å. In the presence of a minimal-length DNA binding sequence (a 24-base-pair duplex DNA), a 1:1 Ku/DNA complex forms. This 1:1 stoichiometry is observed when either the Ku or the DNA is in excess. Analysis of the contrast variation data on Ku complexed with either the 24-mer duplex DNA or a slightly longer 30-mer duplex DNA shows that both the DNA and Ku structures have the same overall conformations within the 1:1 complex as the uncomplexed components. The separation of the centers-of-mass for the Ku/24-mer DNA complex is 46 Å, while that for the Ku/30-mer DNA is 56 Å. The DNA binds within what appears to be a preformed channel that penetrates deeply into the Ku protein such that the entire length of the 24-mer DNA spans the protein. The slightly longer 30-mer binds in a similar fashion, but with its extra length protruding from the protein envelop. The scattering data are consistent with the idea that the Ku "threads" onto the duplex DNA via a channel that can completely bury approximately 24 base pairs.

Double-stranded DNA break repair is required for cellular survival following exposure of cells to ionizing radiation as well as for the normal rearrangement of immunoglobulin and T cell receptor genes [V(D)J recombination] in lymphocytes (*1*−*3*). In mammalian cells, the rejoining of double-stranded DNA breaks requires the activity of the DNA-dependent protein kinase (DNA-PK)[1] (*2, 3*) which is also implicated in the regulation of transcription (*4, 5*). DNA-PK is a nuclear serine/threonine protein kinase that has the unique property of being stimulated by double-stranded DNA (*6, 7*). The DNA-PK holoenzyme is comprised of a 465 kDa catalytic subunit (DNA-PKcs) and a DNA targeting component known as Ku (*8*−*12*). Ku is a heterodimer, having 70 and 83 kDa subunits, that binds to DNA in both sequence-independent and sequence-dependent modes (*5*). DNA sequence-independent binding by Ku requires single-to-double-stranded DNA transitions such as free DNA ends, hairpin loops, single-stranded nicks, or gaps (*13*−*16*), and it is this mode of DNA binding that is proposed to function in double-stranded DNA break repair. It has been suggested that DNA-PK plays both structural and signal transduction roles in repair. Suggested structural roles include protecting, tethering, and/or aligning DNA ends, or possibly providing scaffolding for the assembly of a repair complex (*2, 3, 17*). The mechanism by which double-stranded DNA breaks are repaired in vivo and the precise role of DNA-PK in this process are not known.

There is very little structural data available on DNA-PK or its components, or on the interactions of DNA-PK with DNA. Atomic force microscopy (AFM) has been used to visualize both Ku and DNA-PK in association with DNA (*18*−*20*). The AFM data suggest Ku mediates the formation of DNA loops and end-linked intermolecular DNA complexes. These data were interpreted to indicate that Ku is capable of self-association when bound to DNA and that this self-association tethers the broken DNA strands in preparation for repair. This model is further supported by biochemical data showing Ku stimulates the ligation of DNA molecules by mammalian DNA ligases (*21*).

To shed further light on the biochemical properties of Ku, we undertook small-angle X-ray and neutron scattering studies of Ku and Ku/DNA complexes in solution. These experiments have yielded information on the overall shape of the Ku heterodimer in solution, the stoichiometry of Ku/DNA in specific complexes, and the nature of the interaction

† This work was performed under the auspices of the U.S. Department of Energy (DOE) under contract to the University of California, and was supported by DOE/OBER Project KP1101010 (to J.T.) and by National Institutes of Health Project CA50519 (to D.J.C.). Neutron scattering data were obtained using instruments supported by the National Science Foundation under Agreement DMR-9423101 and the Cold Neutron Research Facility at the National Institutes of Standards.

* Corresponding author. 505-6672031 (Phone), 505-6670110 (FAX), jtrewhella@lanl.gov (E-mail).

‡ Chemical Science and Technology Division.

§ Current address: Solid State Division, Oak Ridge National Laboratory, Oak Ridge, TN 37831.

|| Life Sciences Division.

[1] Abbreviations: AFM, atomic force microscopy; D, deuterium or ^{2}H; d_{max}, maximum linear dimension; DNA-PK, DNA-dependent protein kinase; DNA-PKcs, DNA-PK catalytic subunit; DNA24 or 24-mer DNA, 24-base-pair DNA; DNA30 or 30-mer DNA, 30-base-pair DNA; DTT, dithiothreitol; EDTA, ethylenediaminetetraacetic acid; I_0, forward or zero-angle scattering; H, protium or ^{1}H; HEPES, 4-(2-hydroxyethyl)-1-piperazineethanesulfonic acid; Ku or Ku70/80, the DNA targeting component of DNA-PK; Ku70 and Ku80, the 70 and 83 kDa subunits, respectively, of Ku; R_g, radius of gyration; R_c, radius of gyration of cross section.

10.1021/bi9825246 CCC: $18.00
Published on Web 01/30/1999

between the Ku and DNA components. Neutron scattering with contrast variation was used to determine the overall shapes and dispositions of the Ku and DNA components within Ku/DNA complexes. The scattering experiments utilized relatively short DNA fragments (24- and 30-mer oligomers) having the minimal sequence length that can bind Ku (*7*). Under the experimental conditions used in the solution scattering experiments, association of Ku with DNA does not give rise to any large-scale conformational changes in the enzyme and does not lead to Ku self-associations. Modeling of the scattering data indicates the DNA binds to Ku such that it penetrates the protein by binding to what appears to be a preformed channel. The combined results of the scattering, electron microscopy, and biochemical studies suggest that the ability of Ku to mediate DNA end alignment is not a function of Ku−Ku interactions, but alternatively may involve alteration of DNA end structure resulting in DNA−DNA interactions.

MATERIALS AND METHODS

Preparation of DNA Substrates. Two different double-stranded DNA oligomers were prepared as substrates for Ku: a 24-mer and a 30-mer, with respective single-strand sequences of 5′-GAG CTC GGT ACC CGG GAT CCT CTA-3′ and 5′-AAT TCG AGC TCG GTA CCC GGG ATC CTC TAG-3′. They were synthesized using an Applied Biosystems automated DNA synthesizer and standard phosphoramidite chemistry. The DNA was stored in a buffer containing 50 mM HEPES, pH 7.5, 100 mM KCl, 2 mM EDTA, and 1 mM DTT. The concentrations of DNA solutions were determined initially by UV absorption measurement, $\epsilon_{260} = 735\ M^{-1}\ cm^{-1}$.

Preparation of Ku and Ku/DNA Complexes. Ku was purified from baculovirus-transformed insect cells (*22*). The Ku70/80 heterodimer was purified from Sf9 cells that were coinfected with viruses encoding the Ku70 and Ku80 subunits. The recombinant heterodimer was purified using SP-Sepharose, Q-Sepharose, heparin agarose, and DNA-affinity chromatography (*18*). A Coomassie stain of the Ku protein showed it to be highly pure and present in a 1:1 mixture of Ku70 and Ku80. The final DNA affinity chromatography step would eliminate any small amounts of monomeric Ku70 or Ku80, if present. Gel shift assay data showed a 1:1 complex of Ku with the 24-mer DNA (*18*), as well as with the 30-mer DNA (data not shown). Purified Ku was stored in the same buffer as the DNA. The concentration of the Ku70/80 heterodimer was determined initially by UV absorption measurements using an extinction coefficient $\epsilon_{280} = 79\,460\ M^{-1}\ cm^{-1}$. This extinction coefficient value is estimated using the amino acid sequence of Ku and simply summing the corresponding free amino acid values (*23*). For the X-ray scattering experiments aimed at evaluating how many DNA molecules bind to Ku, and whether Ku self-associates in the presence of DNA, the protein and DNA concentrations of the stock solutions used to prepare Ku/DNA mixtures in precise stoichiometries were checked by analysis of the forward scattering (see below). This method avoids systematic errors arising from contributions to the UV absorption due to the effects of differential oxidation of DTT in the stock solutions and buffers, as well as from the use of calculated extinction coefficients.

Scattering Data Acquisition. X-ray scattering data were collected using the instrument described in Heidorn and Trewhella (*24*). Neutron scattering measurements were collected using the 30-m SANS instrument (NG3) at the National Institute of Standards and Technology (NIST) (*25*) as described in Olah et al. (*27*). Neutrons with a mean wavelength of 5.0 Å were used with a full-width-at-half-maximum (fwhm) of 34%. Sample-to-detector distances of 7.0 and 1.5 m were used to obtain data in the Q-range 0.012−0.35 $Å^{-1}$. Data from two sets of samples, Ku complexed with 24-mer DNA (DNA24) and Ku with the 30-mer DNA (DNA30), were collected. Sample cells were 1-mm path-length quartz cuvettes for samples in buffers with <40% D_2O (0% for Ku/DNA24, 0% and 16% for Ku/DNA30) and 4-mm path-length quartz cuvettes for samples in buffers with higher deuteration levels (70, 85, and 100% for Ku/DNA24; 86 and 100% for Ku/DNA30). Neutron transmissions are higher for these latter samples due to their lower H content. Data were collected at a constant temperature of 13 °C. The protein concentration values for all samples measured with neutrons were ~33 μM (~5 mg/mL).

Scattering Data Analysis. The scattering data were analyzed as previously described (*26*, *27*). The scattering of neutrons (or X-rays) from a homogeneous solution of monodisperse particles (such as proteins, DNA, or their complexes) can be expressed as

$$I(Q) = \langle | \int [\rho(\mathbf{r}) - \rho_s] \exp(-i(\mathbf{Q}\cdot\mathbf{r})\, d\mathbf{r}|^2 \rangle \qquad (1)$$

where $Q = (4\pi \sin \theta)/\lambda$ is the amplitude of the scattering vector (2θ is the scattering angle and λ is the wavelength of the X-rays or neutrons). The difference between the scattering densities for the particle, $\rho(\mathbf{r})$, and solvent, ρ_s, is the "contrast" of the particle. Scattering densities are calculated simply as the sum of the scattering amplitudes per unit volume. For X-rays, the scattering amplitudes are equal to the number of electrons in the atom, while for neutrons scattering lengths are used. The integration is taken over the volume of the particle, and the broken brackets denote the average over all molecule orientations. Molecular volumes were calculated using

$$V = 2\pi^2 I_0 / Q_i \qquad (2)$$

where Q_i is the scattering invariant (*28*):

$$Q_i = \int Q^2 I(Q)\, dQ \qquad (3)$$

The inverse Fourier transform of $I(Q)$ yields $P(r)$, the probable frequency distribution of interatomic vectors within the scattering particle. $P(r)$ functions were calculated using GNOM (*29*). $P(r)$ goes to zero at the maximum linear dimension, d_{max}, of the scattering particle, and its zeroth and second moments give forward scatter, I_0, and radius of gyration, R_g, respectively. An alternative method for calculating R_g and I_0 is to use the Guinier approximation (*30*) which states that for a globular particle, the innermost portion of the scattering profile can be approximated by a Gaussian curve, i.e.:

$$I(Q) = I_0 e^{-(1/3)Q^2 R_g^2} \qquad (4)$$

For a monodisperse solution of identical particles, a plot of log [$I(Q)$] vs Q^2 thus yields R_g and I_0, from the slope and intercept, respectively. When one dimension of a particle is much greater than the other two, e.g., a rod, Guinier (*30*) also showed that one can approximate the smallest-angle scattering as

$$QI(Q) = I_{c0}e^{-(1/2)Q^2R_c^2} \quad (5)$$

where R_c is the radius of gyration of the cross section. For a rod of length L and radius R, $R_c = R\sqrt{2}$, and R_g and R_c are related by

$$R_g^2 - R_c^2 = L^2/2 \quad (6)$$

For particles of the same mean scattering density, I_0 is proportional to the square of their molecular weights and to the particle concentration. Since proteins in general have the same mean scattering density, by using a standard protein of known concentration that is also known to be monodisperse in solution and comparing I_0 values between the protein standard and other monodisperse protein solutions, one can determine protein concentration values very precisely and accurately. Comparison of the forward scattering I_0 of the Ku sample with a lysozyme standard (*31*) was used to obtain accurate concentrations of Ku solutions used in the X-ray scattering experiments. The I_0 values measured for the DNA in solution can also be used to calibrate concentrations providing the contrast difference between the protein and DNA is taken into account. Using the known chemical compositions of Ku and DNA, and assuming typical values for the specific volumes of the protein (~0.74 cm^3/g) and for double-stranded DNA (~0.52 cm^3/g), the electron densities for Ku and DNA were calculated as $\rho_{Ku} = 0.436$ e/Å^{-3} and $\rho_{DNA} = 0.598$ e/Å^{-3}, respectively. The electron density of the solvent is $\rho_s = 0.335$ e/Å^{-3}; hence, the contrast for DNA ($\Delta\rho_{DNA} = 0.264$ e/Å^{-3}) is ~2.6 times that of Ku ($\Delta\rho_{Ku} = 0.101$ e/Å^{-3}). Concentration values for the DNA were calculated using this contrast ratio and the molecular mass for the DNA24 (14.7 kDa).

Contrast variation (*32*, *33*) is a powerful tool that, in the case of neutron scattering from protein/DNA complexes, takes advantage of the natural difference in the mean neutron scattering densities for proteins and DNA, both of which lie between those values for H_2O and D_2O. By varying the D_2O:H_2O ratio in the solvent, one can vary the relative contrasts of the DNA and protein components, and hence their contributions to the total scattering (eq 1). From a series of measurements at different contrast values, information on the conformations and dispositions of the DNA and protein within a complex can be obtained. Assuming internal scattering density fluctuations are negligible, the total scattering from a DNA/Ku complex can be written as

$$I(Q,\Delta\rho_{DNA},\Delta\rho_{Ku}) = \Delta\rho_{DNA}^2 I_{DNA}(Q) + \Delta\rho_{DNA}\Delta\rho_{Ku}I_{DNA,Ku}(Q) + \Delta\rho_{Ku}^2 I_{Ku}(Q) \quad (7)$$

where $\Delta\rho_{DNA}$ equals $\rho_{DNA} - \rho_S$ and ρ_{DNA} is the mean scattering density for DNA. A similar definition holds for $\Delta\rho_{Ku}$. The three basic scattering functions in eq 7 are $I_{DNA}(Q)$, and $I_{Ku}(Q)$, representing the scattering due to the DNA and Ku, and $I_{DNA,Ku}(Q)$, which is the cross-term that gives information on the relative dispositions of the DNA and Ku components. The inverse Fourier transform of the basic scattering functions gives the distribution of vector lengths, $P(r)$, between scattering centers within the DNA and Ku components, as well as those between the DNA and Ku, respectively. The first moment of the $P(r)$ calculated from the cross-term approximates the separation of the centers of mass for a two-component complex.

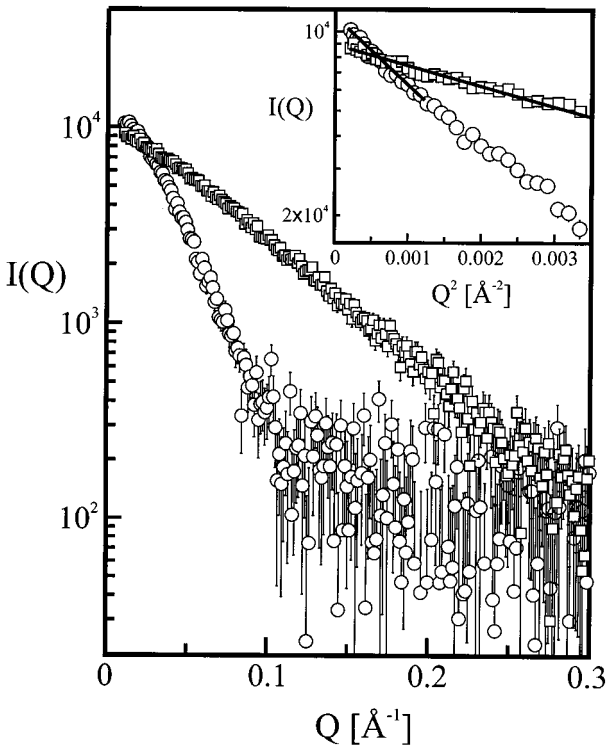

FIGURE 1: X-ray scattering data for Ku (○) and DNA (□). The insert shows the respective Guinier plots.

Modeling the Scattering Data. A Monte Carlo simulation program, SASMODEL (*34*), was used to model the scattering data. The program is designed to find the shapes and relative dispositions of macromolecular components (domains, subunits) that best fit the experimental scattering data. An ellipsoid was used to represent the Ku70/80 protein while a cylinder with dimensions approximating a double-stranded DNA structure was used to model the DNA. The program generates ellipsoids and/or cylinders with specific sizes and locations and fills these shapes with random points. $P(r)$ is calculated by summing all pairwise combinations of these points weighted by the product of the scattering densities. $I(Q)$ functions are calculated as the inverse Fourier transform of the model $P(r)$ using the same Q-range as the experimental data to facilitate comparison. Both $I(Q)$ and $P(r)$ are compared with the experimental data by means of least-squares methods. These calculations can be done very rapidly, thus enabling extensive searches of conformational space. For the modeling presented here, a global minimization routine was used to find the best-fit model (*35*). The use of appropriate constraints with this modeling approach can facilitate finding best-fit models to scattering data with a high level of confidence (*34*, *36*−*39*).

RESULTS

X-ray Scattering Results for Free Ku and DNA: Shape Analysis. Figure 1 shows X-ray scattering data for free Ku

Table 1: Structural Parameters for Ku and for Ku/DNA24 Mixtures from X-ray Scattering Measurements[a]

Ku:DNA mole ratio	R_g (Å)	d_{max} (Å)	$I_{0(Ku+DNA)}/I_{0(DNA)}$[b]	$I_{0(Ku+DNA)}/I_{0(Ku)}$[b]
DNA24 (0:1)	24.6 ± 0.3	85	1	–
1.06:1	49.9 ± 1.6	170	22.44 ± 0.96	1.34 ± 0.09
2.11:1	48.2 ± 0.8	170	42.43 ± 1.23	1.27 ± 0.06
KU70/80 (1:0)	50.0 ± 1.2	170	–	1
1:1.89	50.6 ± 0.9	175	12.80 ± 0.42	1.53 ± 0.08
1:3.79	49.2 ± 0.6	170	6.83 ± 0.17	1.63 ± 0.08
1:7.58	46.1 ± 0.8	170	3.96 ± 0.12	1.89 ± 0.10
1:15.16	38.8 ± 1.5	160	2.48 ± 0.08	2.37 ± 0.12

[a] The Ku and DNA concentrations used to calculate mole ratios were obtained using I_0 values calibrated to a lysozyme standard (see Experimental Methods). The total Ku/DNA concentration values for all samples are in the range 1.3−3.4 mg/mL. R_g and d_{max} values are calculated using *P(r)* functions from GNOM. Note that for the samples with a large excess of DNA (≥8-fold) the measured R_g values begin to decrease because the smaller free DNA molecules begin to contribute to the average R_g measured by the scattering experiment. [b] I_0 values are normalized to the molar DNA concentration. [c] I_0 values are normalized to the molar Ku concentration.

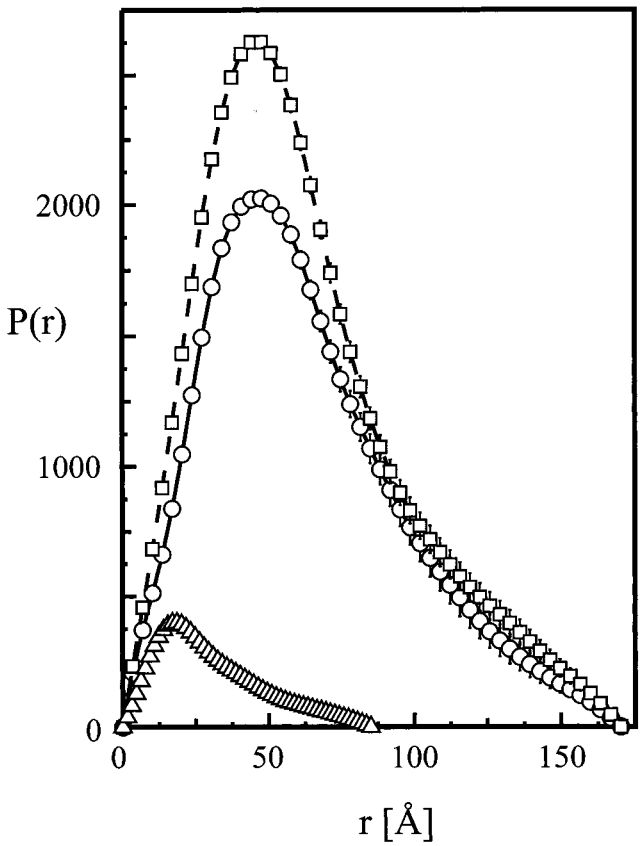

FIGURE 2: *P*(*r*) functions for Ku (○), DNA (△), and Ku/DNA (1:1) (□) calculated from X-ray scattering data. All scattering data are scaled to the molecular weight of respective molecule.

and free DNA24. The derived structural parameters are given in Table 1. The Guinier plots for Ku and DNA show the expected linearity for monodisperse solutions (Figure 1, insert). The calculated volume for the free Ku using eq 2 is $(2.0 \pm 0.2) \times 10^5$ Å^3, in excellent agreement with the value expected for a single Ku70/80 heterodimer (1.9×10^5 Å^3). The *P*(*r*) function for Ku (Figure 2) shows a peak at ∼45 Å and extends to a d_{max} of ∼170 Å, indicating an asymmetric structure. The Ku scattering profile was modeled as an ellipsoid against the scattering data, and the best-fit model (with root-mean-squared deviation of $\chi = 1.2$) was obtained for a prolate ellipsoid with semi-axis lengths ∼24, 43, and 89 Å.

The volume calculated for the DNA from the scattering data using eq 2 is $(1.9 \pm 0.1) \times 10^4$ Å^3, which is 40% larger than the expected value of 1.3×10^4 Å^3 for a double-stranded DNA 24-mer calculated using the specific volume for DNA (0.52 cm^3/g). This larger volume calculated for the highly charged DNA is expected because of the contributions of hydration layer effects (*40*). These effects are also evident in the radius of gyration of cross section (R_c) and d_{max} values determined. The R_c value for the DNA was determined by Guinier analysis (eq 5) to be 7.7 ± 0.1 Å, corresponding to a cross-sectional diameter of 22 Å. The *P*(*r*) function shows a classic rod shape with a peak at ∼20 Å and a d_{max} value of 85 Å (Figure 2). In addition, the measured R_g value for the free 24-mer DNA (25.0 ± 0.6 Å) is in agreement with the value expected for a rod-shaped particle with these approximate dimensions (eq 6). The parameters determined from the scattering data all indicate a rod-shaped particle with dimensions that are slightly larger than those expected for double-stranded DNA (∼20 Å in diameter and 82 Å, using 3.4 Å per base pair in length). A 1−2 Å hydration layer would give the observed ∼40% increased apparent volume for this particle. The scattering data therefore are consistent with the Ku sample being a monodisperse solution of 70/80-heterodimers, and the 24-base-pair DNA being a monodisperse double-stranded duplex DNA.

X-ray Scattering Results from Ku/DNA Complexes: Binding Stoichiometries. X-ray scattering data from six Ku/DNA24 mixtures were measured to determine the stoichiometry of binding. Mixtures were made with Ku:DNA24 ratios ranging from 2:1 to 1:16, and Table 1 gives the I_0 data as well as the R_g and d_{max} values determined. In Figure 3 the measured I_0 values are plotted as a function of the Ku:DNA ratio (left) and the DNA:Ku ratio (right) in the mixtures. The I_0 values are normalized by the molar concentration of DNA (left) or of Ku (right). The I_0 value for a 1:1 complex of Ku and DNA would be proportional to $(\Delta\rho_{Ku}M_{Ku} + \Delta\rho_{DNA}M_{DNA})^2$, whereas in an uncomplexed mixture I_0 would be proportional to the significantly smaller $[(\Delta\rho_{Ku}M_{Ku})^2 + (\Delta\rho_{DNA}M_{DNA})^2]$. M_{Ku} and M_{DNA} are the molecular weight values for Ku and DNA, respectively. Intermediate levels of complex formation would give intermediate I_0 values. For a mixture of Ku/DNA complex with either excess free DNA or excess free Ku, the I_0 values are proportional to the concentration-weighted average of the expected I_0 values for the complex and the free components. Thus, the I_0 values are very sensitive to the degree of complex formation. To aid in the interpretation of the I_0 data,

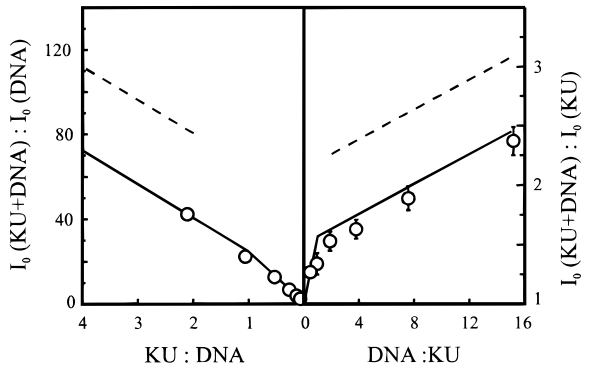

FIGURE 3: Titration of Ku with DNA24. Left: Ratios of I_0 values measured for Ku+DNA24 mixtures to the I_0 value expected for a single DNA molecule, normalized to the DNA concentration, as a function of the Ku:DNA24 mole ratio in the mixture. Right: Ratios of I_0 values for Ku+DNA24 mixtures to the I_0 value expected for a single Ku molecule, normalized to the Ku concentration, as a function of Ku:DNA24 ratio in the mixture. The solid lines are the expected I_0 ratios when one DNA is bound per Ku, while the dashed lines are for two DNA bound to one Ku.

we have plotted in Figure 3 the expected I_0 values for the Ku/DNA mixtures assuming 1:1, 2:1 (Figure 3, left), and 1:2 (Figure 3, right) binding stoichiometries. All of the experimental data fall on the calculated line for a 1:1 Ku:DNA binding stoichiometry, and this binding stoichiometry remains unchanged regardless of whether there is excess Ku or excess DNA. Binding of DNA to Ku did not result in significant changes in R_g, d_{max}, or the shape of the *P(r)* profile (Table 1 and Figure 2), indicating that the DNA binds so as to form a compact complex and there is little change in the overall conformation of Ku.

Neutron Scattering Results for the Ku/DNA Complex: Conformations of the Components and Their Relative Dispositions. Neutron scattering data were collected for the Ku/DNA24 complex in solvents with four different buffer deuteration levels between 0 and 100% (Figure 4A, Table 2). To calculate the basic scattering functions, the contrasts of the Ku and DNA components were calculated using the same procedure as for the X-ray scattering experiment except the neutron scattering lengths were used instead of the number of electrons in each atom. Using the calculated contrast values, the neutron contrast data can be expressed as a set of linear equations of the form of eq 7 that can then be solved for the basic scattering functions. In addition to the neutron contrast data, we also used X-ray scattering of the Ku/DNA24 complex as an additional contrast point to improve the quality of the resulting basic scattering functions. The X-ray data were scaled to the neutron data using I_0 values and the calculated contrasts of Ku and DNA24. The $P(r)$ functions calculated from the respective basic scattering functions are shown in Figure 5A. The $P(r)$ function of the DNA24 obtained from its basic scattering function is in excellent agreement with that obtained from X-ray measurement of the free DNA, indicating that the DNA24 does not change its rodlike shape upon binding to Ku. The $P(r)$ function for Ku calculated from its basic scattering function also agrees well with that of the free Ku measured by X-ray scattering. There are small deviations between the $P(r)$ functions for free Ku and Ku in the complex which might be attributed to subtle conformational changes within Ku when it binds the DNA24; however, there are no large-scale conformational changes. Using the first moment of the Ku/DNA24 cross-term, the center-of-mass separation between Ku and DNA24 within the complex is estimated to be 46 ± 6 Å.

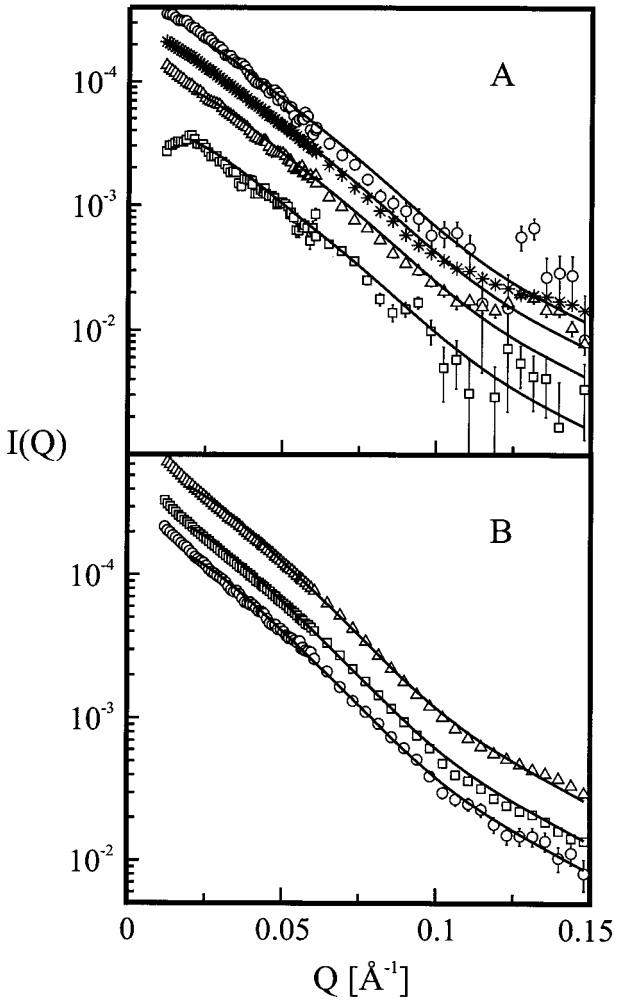

FIGURE 4: Neutron contrast data of the Ku/DNA24 and Ku/DNA30 complexes with different levels of buffer deuteration. (A) Ku/DNA24 in 0% D_2O (○), 70% D_2O (□), 85% D_2O (△), or 100% D_2O (∗). (B) Ku/DNA30 in 16% D_2O (○), 86% D_2O (□), or 100% D_2O (△). The solid lines are calculated model scattering profiles calculated for the models in Figure 6 using the Monte Carlo simulation (see Materials and Methods).

Table 2: Neutron Contrast Data for Ku/DNA Complexes with 24- and 30-mer DNA

	buffer deuteration (%)	R_g (Å)
Ku/DNA24	0	54.8 ± 0.9
	70	51.3 ± 4.6
	85	50.9 ± 1.2
	100	54.0 ± 0.2
Ku/DNA30	16	56.3 ± 0.2
	86	54.7 ± 0.3
	100	53.8 ± 0.3

[a] The total Ku+DNA concentration values for all samples are in the range ~2−7 mg/mL. R_g values are calculated from the *P(r)* functions using GNOM. The neutron-derived R_g values reflect the changing contrasts of the DNA and Ku components with different deuteration levels in the buffer.

We also measured a neutron contrast series for a Ku/DNA30 complex. Three different solvent deuteration levels were used (Table 2, Figure 4B), and these data combined with X-ray scattering data from the same complex gave a

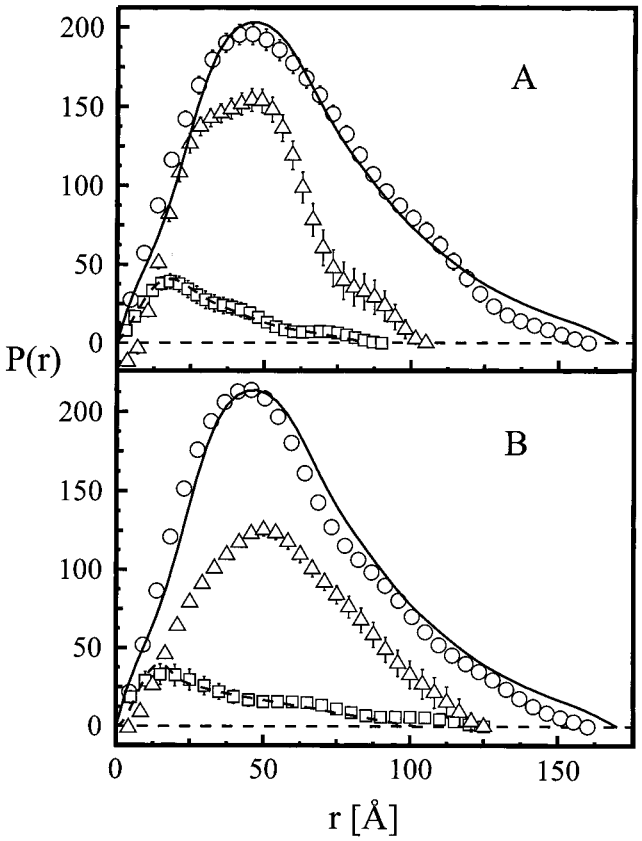

FIGURE 5: *P*(*r*) functions derived from the basic scattering functions for the Ku/DNA24 and Ku/DNA30 complexes. (A) Ku/DNA24 complex: Ku (○), DNA (24mer) (△), and Ku−DNA cross-term (□). (B) Ku/DNA30 complex: Ku (○), DNA (30mer) (△), and Ku−DNA cross-term (□). For comparison, the *P*(*r*) functions of the free Ku (—, in A and B), DNA (24mer) (---, in A) measured using X-rays, and the calculated *P*(*r*) function of a rod 102 Å in length and 22 Å in cross-section diameter (- - -, in B) are also shown. All data are scaled to the molecular weight of respective molecule.

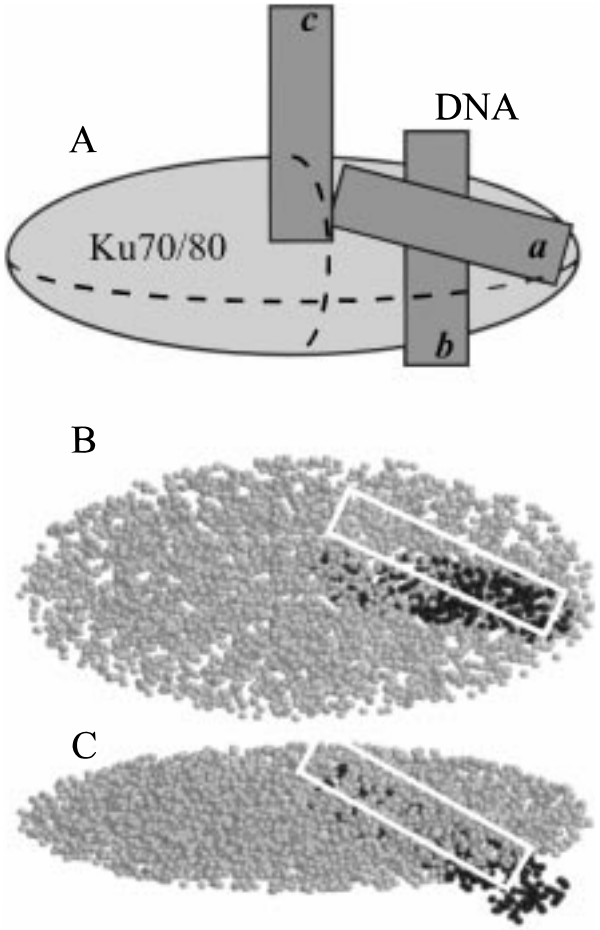

FIGURE 6: Models of the Ku+DNA24 and Ku+DNA30 interactions. (A) Illustration of three possible modes of interaction between the Ku70/80 heterodimer and DNA. The Ku protein is represented by the ellipsoid shape, and three alternative DNA orientations are indicated by the rectangular shapes labeled *a*, *b*, or *c*. (B, C) Two views of the Ku+DNA24 binding model as obtained by the Monte Carlo simulation (see Materials and Methods). The two views are obtained by a 90° rotation about the horizontal ellipsoid axis. Ku is represented by the ellipsoid filled with gray spheres, while the DNA is represented by the rod shape filled with black spheres. The white rectangles indicate the uncertainty of the DNA binding site as evaluated by inspection of the close-to-best-fit models (see Results).

total of four contrast measurements from which the basic scattering functions were extracted in a manner similar to those for Ku/DNA24. The *P*(*r*) functions calculated from the basic scattering functions derived for the Ku/DNA30 complex (Figure 5B) agree well with those determined for the Ku/DNA24 complex. Again there is little change in the Ku shape upon DNA binding. Further, the DNA30 has an approximately rod-shaped structure with the same cross-sectional radius as the DNA24, as evidenced by the peaks in their respective *P*(*r*) functions being at the same values. The d_{max} value for the DNA30 is longer than that for DNA24 by 20 Å (d_{max} = 105 Å) as expected for a double-stranded DNA structure having an additional 6 base pairs (3.4 Å/bp). The first moment of the *P*(*r*) function calculated for the Ku/DNA30 cross-term gives a center-of-mass separation between the Ku and DNA30 components in this complex of 56 ± 7 Å.

Modeling the Ku and DNA Components within the Ku/DNA Complex. Since there is a finite and significant separation of the centers of mass for the DNA and protein components in both the Ku/DNA24 and Ku/DNA30 complexes, we know that the DNA must be bound asymmetrically to the Ku70/80 heterodimer. In Figure 6A, three distinctive DNA binding modes are shown, each of which has a center-of-mass separation for the Ku and DNA components between 46 and 56 Å. The binding mode depicted as *c* seems most unlikely. It has been shown previously by DNase footprinting that the Ku70/80 heterodimer protects approximately 30 bp of double-stranded DNA (*7*) and for binding mode *c* more than half the DNA bases would not interact with the Ku protein. For binding mode *c*, one would expect the minimal binding DNA sequence therefore would be approximately half as long. The binding modes depicted as *a* and *b* both show extensive contacts along most of the length of the DNA. However, the fact that the center-of-mass separation between Ku and the 30-mer DNA is approximately 10 Å longer than that between Ku and the 24-mer DNA favors binding mode *a*.

To test all possible binding modes for the DNA with respect to the Ku, we modeled the neutron contrast data of the Ku/DNA24 using SASMODEL (see Materials and Methods). The Ku was modeled as a single ellipsoid and the DNA24 as a rod. The three semi-axes of the ellipsoid were constrained to ±2 Å of the values derived by modeling

the Ku basic scattering function, which are essentially the same as the values for Ku free in solution. The rod-shaped DNA was constrained to be 22 ± 1 Å in diameter of cross section and 82 ± 2 Å in length. The center-of-mass separation between the Ku and DNA components was constrained to the range of values obtained from the cross-term basic scattering function (46 ± 6 Å). There were no other constraints on the relative disposition of Ku and DNA; i.e., the relative orientations of the Ku and DNA components were completely free. Figure 6 (B and C) shows two views of the resultant Ku and DNA24 dispositions in the best-fit model. The 24-mer DNA penetrates the Ku ellipsoid, and there are interactions between almost the full length of the DNA and about half of the Ku70/80 heterodimer. The center-of-mass separation between the Ku and DNA components is 42 Å. This binding mode agrees with that depicted as *a* in Figure 6A. When examining the close-to-best-fit models obtained by the Monte Carlo simulation, we found that all these models agree with the best-fit model but with some variation in the precise orientation of the 24-mer DNA with respect to the Ku ellipsoid axes and the extent of the interaction (see Figure 6B,C). The essential insight into the Ku−DNA interaction obtained from the modeling is that the DNA24 interacts with Ku extensively, apparently penetrating the Ku ellipsoid such that it sits within a channel. This channel appears to allow the DNA to "thread" through the Ku structure as the best-fit model, as well as the consensus of the close-to-best-fit models, has the DNA approximately spanning the Ku ellipsoid. Since no large-scale conformational change of Ku is observed upon Ku/DNA complex formation, this channel appears to be preformed. DNA oligomers shorter than 24 bp would not be able to interact to the same extent with the channel, and thus would be predicted to have a weaker interaction. The model thus supports the fact that the 24-mer is the shortest sequence that binds tightly to Ku. The calculated scattering for the model in Figure 6B,C is shown in comparison to the experimental data in Figure 4A.

The same modeling procedure as described above for the Ku/DNA24 was used to model the Ku/DNA30 neutron contrast data. The modeling conditions were the same as for the Ku/DNA24 data except the length of the DNA was set to 102 ± 2 Å and the center-of-mass separation between Ku and DNA was set to 56 ± 7 Å. The resultant best-fit models resemble the Ku/DNA24 model in Figure 6, with some extra length of the 30-mer DNA sticking out of the Ku ellipsoid (model not shown). The center-of-mass separation between Ku70/80 and DNA30 is 50 Å in the best-fit model. When compared with the model obtained for the Ku/DNA24 complex, the DNA binding position on Ku and the relative orientation between Ku and DNA are quite similar. This result is remarkable because the two model searches were quite independent with no constraints requiring similar interactions.

DISCUSSION

Using small-angle scattering data, we have shown that the Ku70/80 heterodimer is highly asymmetric. Its longest and shortest dimensions are ∼180 Å and ∼50 Å. The modeling of the neutron contrast variation data indicates that in the 1:1 Ku/DNA complexes, the DNA interacts with its full length occupying a channel that spans the Ku70/80 heterodimer. Since the Ku70 and Ku80 subunits of Ku are close to equal in size, approximately half the ellipsoid volume of our Ku ellipsoid model will be occupied by each subunit. With the current scattering data, however, we cannot assign which part of the Ku ellipsoid is occupied by which subunit. From biochemical studies, we know that Ku70 can bind to DNA in the absence of the Ku80 (*41*) through a mechanism that is sensitive to removal of nine amino acids from the C-terminus (*42*). The affinity of the Ku70 subunit with DNA appears to be lower than the Ku70/80 complex and does not result in a detectable gel mobility shift in native electrophoresis (*42*). Also, removal of the C-terminal DNA binding domain of the Ku70 subunit does not affect the ability of the Ku70/80 complex to bind to DNA or function in DNA double-strand break repair (*43*). A detailed analysis of Ku70/80 interactions indicates the association of Ku80 with Ku70 induces a mode of DNA binding that is sensitive to truncations at the N-terminus of Ku70 (*43, 44*). These data suggest that the DNA binding activity of the Ku70/80 heterodimer requires both subunits. One interpretation of the data is that the DNA binding cleft of the Ku70/80 complex is composed of protein domains donated by both the Ku70 and Ku80 subunits. Alternatively, the dimerization of the two Ku subunits may result in a conformational change in one of the subunits that creates a DNA binding site. In either case, the scattering data are consistent with the idea that the Ku70/86 complex "threads" onto DNA via a channel that can completely bury a 24-base-pair duplex DNA. The concept of Ku threading onto DNA was first proposed by Paillard and Strauss (*45*), who showed that, unlike Ku bound to linear DNA, Ku complexes "trapped" on recircularized DNA are resistant to dissociation by high ionic strength buffers.

The scattering data also show that there is no Ku self-association either in the absence or in the presence of the minimal length Ku binding DNA oligomers. For the shortest DNA sequence (24−mer) that binds to Ku, the binding stoichiometry between Ku and DNA is 1:1 regardless of whether Ku or DNA is in excess in the sample. The capacity for Ku70/80 to stimulate the end-association of DNA fragments observed by AFM (*18*) therefore seems unlikely to be mediated by Ku−Ku interactions and may require DNA fragments longer than those used in the experiments described in this report. One intriguing possibility is that the ability of Ku to stimulate DNA end-linking is not a function of protein−protein interactions, but is instead mediated by changes in the structure of the ends of the DNA molecules that favor the formation of DNA−DNA interactions.

REFERENCES

1. Alt, F. W., Oltz, E. M., Young, F., Gorman, J., Taccioli, G., and Chen, J. (1992) *Immunol. Today 13*, 306−314.
2. Jackson, S. P., and Jeggo, P. A. (1995) *Trends Biochem. Sci. 20*, 412−415.
3. Jeggo, P. A., Taccioli, G. E., and Jackson, S. P. (1995) *Bioessays 17*, 949−957.
4. Dynan, W. S., and Yoo, S. (1998) *Nucleic Acids Res. 26*, 1551−1559.
5. Giffin, W., Torrance, H., Rodda, D. J., Prefontaine, G. G., Pope, L., and Hache, R. J. G. (1996) *Nature 380*, 265−268.
6. Anderson, C. W., and Lees-Miller, S. P. (1992) *Crit. Rev. Eukaryotic Gene Expression 2*, 283−314.
7. Gottlieb, T. M., and Jackson, S. P. (1993) *Cell 72*, 131−142.

8. Leesmiller, S. P., Chen, Y. R., and Anderson, C. W. (1990) *Mol. Cell. Biol. 10*, 6472−6481.
9. Carter, T., Vancurova, I., Sun, I., Lou, W., and Deleon, S. (1990) *Mol. Cell. Biol. 10*, 6460−6471.
10. Dvir, A., Peterson, S. R., Knuth, M. W., Lu, H., and Dynan, W. S. (1992) *Proc. Natl. Acad. Sci. U.S.A. 89*, 11920−11924.
11. Dvir, A., Stein, L. Y., Calore, B. L., and Dynan, W. S. (1993) *J. Biol. Chem. 268*, 10440−10447.
12. Hartley, K. O., Gell, D., Smith, G. C. M., Zhang, H., Divecha, N., Connelly, M. A., Admon, A., Leesmiller, S. P., Anderson, C. W., and Jackson, S. P. (1995) *Cell 82*, 849−856.
13. Morozov, V. E., Falzon, M., Anderson, C. W., and Kuff, E. L. (1994) *J. Biol. Chem. 269*, 16684−16688.
14. Blier, P. R., Griffith, A. J., Craft, J., and Hardin, J. A. (1993) *J. Biol. Chem. 268*, 7594−7601.
15. Griffith, A. J., Blier, P. R., Mimori, T., and Hardin, J. A. (1992) *J. Biol. Chem. 267*, 331−338
16. Mimori, T., and Hardin, J. A. (1986) *J. Biol. Chem. 261*, 375−379.
17. Roth, D. B., Lindahl, T., and Gellert, M. (1995) *Curr. Biol. 5*, 496−499.
18. Cary, R. B., Peterson, S. R., Wang, J. T., Bear, D. G., Bradbury, E. M., and Chen, D. J. (1997) *Proc. Natl. Acad. Sci. U.S.A. 94*, 4267−4272.
19. Yaneva, M., Kowalewski, T., and Lieber, M. R. (1996) *EMBO J. 16*, 5098−5112.
20. Pang, D. L., Yoo, S., Dynana, W. S., Jung, M., and Dritschilo, A. (1997) *Cancer Res. 57*, 1412−1415.
21. Ramsden, D. A., and Gellert, M. (1998) *EMBO J. 17*, 609−614.
22. Ono, M., Tucker, P. W., and Capra, J. D. (1994) *Nucleic Acids Res. 22*, 3918−3924.
23. Gill, S. C., and Von Hippel, P. H. (1989) *Anal. Biochem. 182*, 319−326.
24. Heidorn, D. B., and Trewhella, J. (1988) *Biochemistry 27*, 909−915.
25. Hammouda, B., Barker, J. G., and Krueger, S. (1996) *Small Angle Neutron Scattering Manuals*, NIST, Gaithersburg, MD.
26. Heidorn, D. B., Seeger, P. A., Rokop, S. E., Blumenthal, D. K., Means, A. R., Crespi, H., and Trewhella, J. (1989) *Biochemistry 28*, 6757−6764.
27. Olah, G. A., Rokop, S. E., Wang, C. L. A., Blechner, S. L., and Trewhella, J. (1994) *Biochemistry 33*, 8233−8239.
28. Porod, G (1982) in *Small-Angle X-ray Scattering*, pp 17−51, Academic Press, New York.
29. Svergun, D. I., Semenyuk, A. V., and Feigin, L. A. (1988) *Acta Crystallogr., Sect. A: Fundam. Crystallogr. A44*, 244−250.
30. Guinier, A. (1939) *Ann. Phys. (Paris) 12*, 161−237
31. Krigbaum, W. R., and Kugler, F. R. (1970) *Biochemistry 9*, 1216−1223.
32. Ibel, K., and Stuhrmann, H. B. (1975) *J. Mol. Biol. 93*, 255−265.
33. Moore, P. B. (1981) *J. Appl. Crystallogr. 14*, 237−240.
34. Zhao, J., Hoye, E., Boylan, S., Walsh, D. A., and Trewhella, J. (1998) *J. Biol. Chem. 273*, 30448−30459.
35. Ingber, L. (1993) *URL http://www.ingber.com/#ASA-CODE*, Global optimization C-code, Lester Ingber Research, Chicago, IL.
36. Olah, G. A., and Trewhella, J. (1994) *Biochemistry 33*, 12800−12806.
37. Krueger, J. K., Olah, G. A., Rokop, S. E., Zhi, G., Stull, J. T., and Trewhella, J. (1997) *Biochemistry 36*, 6017−6023.
38. Krueger, J. K., Zhi, G., Stull, J. T., and Trewhella, J. (1998) *Biochemistry 37*, 13997−14004.
39. Olah, G. A., Gray, D. M., Gray, C. W., Kergil, D. L., Sosnick, T. R., Mark, B. L., Vaughan, M. R., and Trewhella, J. (1995) *J. Mol. Biol. 249*, 576−594.
40. Zaccai, G., and Jacrot, B. (1983) *Annu. Rev. Biophys. Bioeng. 12*, 139−157.
41. Wang, J., Satoh, M., Chou, C. H., and Reeves, W. H. (1994) *FEBS Lett. 351*, 219−224.
42. Chou, C. H., Wang, J., Knuth, M. W., and Reeves, W. H. (1992) *J. Exp. Med. 175*, 1677−1684.
43. Wang, J., Dong, X., Myung, K., Hendrickson, E. A., and Reeves, W. H. (1998) *J. Biol. Chem. 273*, 842−848.
44. Jin, S., and Weaver, D. T. (1997) *EMBO J. 16*, 6874−6885.
45. Paillard, S., and Strauss, F. (1991) *Nucleic Acids Res. 19*, 5619−5624.

BI9825246